

# Assessing Protein Loop Flexibility by Hierarchical Monte Carlo Sampling

Jerome Nilmeier,<sup>†,§</sup> Lan Hua,<sup>†,§</sup> Evangelos A. Coutsiyas,<sup>‡</sup> and Matthew P. Jacobson<sup>\*,†</sup>

<sup>†</sup>Department of Pharmaceutical Chemistry, University of California in San Francisco, San Francisco, California 94158-2517, United States

<sup>‡</sup>Department of Mathematics and Statistics, University of New Mexico, Albuquerque, New Mexico 87131, United States

**ABSTRACT:** Loop flexibility is often crucial to protein biological function in solution. We report a new Monte Carlo method for generating conformational ensembles for protein loops and cyclic peptides. The approach incorporates the triaxial loop closure method, which addresses the inverse kinematic problem for generating backbone move sets that do not break the loop. Side chains are sampled together with the backbone in a hierarchical way, making it possible to make large moves that cross energy barriers. As an initial application, we apply the method to the flexible loop in triosephosphate isomerase that caps the active site and demonstrate that the resulting loop ensembles agree well with key observations from previous structural studies. We also demonstrate, with three other test cases, the ability to distinguish relatively flexible and rigid loops within the same protein.

## 1. INTRODUCTION

A great deal of effort has been directed toward the development of computational methods for predicting the conformations of protein loops, which is a critical task in comparative protein modeling and in computational protein design.<sup>1–4</sup> The success of these methods has been evaluated primarily by comparing the results of the loop predictions with the loop conformations observed in crystal structures. That is, the focus is predicting the structure of the loop—a specific conformation—rather than the ensemble of conformations populated under biologically relevant conditions. Although these loop prediction methods can be used to identify multiple low-energy conformations, it is challenging to determine populations of the conformations, i.e., to relate energies of individual conformations to free energies of micro- or macrostates in the ensemble, although significant progress in this regard has been made by Meirovitch and co-workers.<sup>5–7</sup>

The flexibility of loops, i.e., the ability to adopt multiple conformations at relevant temperatures, is often critical to biological function, by playing an important role in molecular recognition. For example, the active site loop of the triosephosphate isomerase (TIM barrel) changes its conformation from an open to a closed state after binding of the ligands.<sup>8,9</sup> In kinases, two critical loops near the active site are flexible, with important implications for drug discovery: the glycine-rich loop (also called the P-loop) and the activation loop, including the DFG motif, which can adopt at least two major conformations in some kinases, referred to as “out” and “in”. For example, while c-Src generally adopts the DFG-in conformation, the unfavorable DFG-out conformation can be induced by binding small molecules.<sup>10</sup> Loop flexibility can also play an important role in antibody–antigen recognition. The H3 loop in the complementarity-determining region of antibodies, which has the most diversity in sequence and is the most critical loop for antigen affinity and specificity, frequently demonstrates evidence of conformational flexibility.<sup>11–13</sup>

More broadly, there are many cases where loops adopt different conformations in different crystal structures, e.g., holo vs apo, or even different crystal unit cells for the same protein.<sup>14</sup> Although the B factors in crystal structures provide some information about conformational flexibility, each structure is best viewed as a snapshot from the equilibrium ensemble. NMR experiments can provide some direct information about conformational equilibria but generally cannot provide complete information about the ensemble of interconverting structures.

Molecular dynamics (MD) has been widely used to study protein flexibility, including loop dynamics.<sup>15,16</sup> The main liability of MD is that the time scales for interconverting between loop conformations can be long relative to the femtosecond time steps used, such as the millisecond time scale for the TIM capping loop to interconvert between the open and closed states.<sup>17</sup> Although such time scales may soon become accessible by MD simulation, they will remain extremely computationally expensive. Methods like replica exchange MD can be used to accelerate convergence but are likewise computationally expensive.

Here, we describe a Monte Carlo method for generating ensembles of loop conformations and cyclic peptides. It is related to classes of loop prediction methods that use torsion-angle sampling of backbone and side chain degrees of freedom (DoF), which makes it possible to make large conformational moves that cross energy barriers. Specifically, it builds on loop prediction methods that exploit “inverse kinematics” methods for creating move sets that do not “break” the loop.<sup>18–24</sup> The new contribution here is implementing these moves in a Monte Carlo scheme that also samples side chain DoF.<sup>25</sup> We apply the method to a number of proteins with flexible loops, including the well-known case of TIM. We also evaluate our ability to distinguish between (relatively) rigid and flexible loops within the same protein.

**Received:** November 18, 2010

**Published:** April 05, 2011

## 2. THE MOVE SET: TORSIONAL PERTURBATIONS VIA INVERSE KINEMATICS

**2.1. Torsions and Sterics.** It is widely accepted that the essential dynamics of a protein backbone can be captured by moves involving only the torsions  $\phi, \psi$  with the other internal variables (bond lengths, bond angles, and  $\omega$  torsions) being kept close to their canonical values, although not necessarily rigid.<sup>19,23,24</sup>

Compared to the high energy associated with  $\omega$  angle deformation,  $\phi$  and  $\psi$  angles are relatively free to rotate, but their range is restricted by steric interactions. Ramachandran regions in the  $(\phi, \psi)$  coordinates for each peptide ensure intrapeptide steric avoidance, and additional restrictions are imposed by more distant clashes. Clashes involving backbone atoms (or atoms bonded to them) are completely determined from the backbone angles. On the other hand, atoms further along side chains (from the  $\gamma$  position out) are not completely determined from the backbone, although their placement may be restricted by it. Significantly, side chains may interact with other side chains so that their placement must be accomplished as a whole. Given a backbone conformation, a separate search is required to determine sterically acceptable or otherwise energetically viable side chain conformations. Reciprocally, backbone moves may be restricted by fixed side chain geometry.

**2.2. MC Move and State Variables.** To design a Monte Carlo move for reversibly exploring the torsion space, we must therefore consider the state space as the set of all torsions,  $\{t_i; \chi_j\}$  where the  $t_i$  are backbone torsions and  $\chi_j$  are side chain torsions, with the indices running respectively over all of the backbone and side chain DoF. A chain of  $\{N, C\alpha, C\}$  triplets (a standard backbone) is one possibility, but chains through, e.g., cysteine bridges, or other macromolecules, such as nucleic acids, could also be considered. In the following, we will assume the standard case (protein backbone loops) exclusively. For the case of a loop of  $N$  residues bridging two fixed ends, the essential backbone DoF would be  $M = 2N - 6$ . Here, six backbone DoF are involved in placing the end of the loop in a fixed rotation/translation relationship to the beginning. We call these DoF, labeled arbitrarily as  $t_i$  ( $i = 1, \dots, 6$ ), the compensators. The remaining  $M$  DoF, labeled as  $t_{\nu}$  ( $\nu = 7, \dots, 2N$ ), are the controls. This separation in controls and compensators is arbitrary and may change from one move to the next. We could assume that the end residues 0 and  $N + 1$  act as hinges; i.e., the  $\phi_0$  and  $\psi_{N+1}$  torsions are fixed, but  $\psi_0, \phi_{N+1}$  are free, adding two DoF to the backbone. The treatment is essentially the same, replacing  $M$  by  $M + 2$  and redefining some indices. We will only discuss the first case (no hinge mobility). It will be assumed that there are  $K$  side chain DoF in the set  $\mathcal{S}$  of side chains interacting with the loop; we may only wish to include in  $\mathcal{S}$  those side chains on the loop and hinges. The placement for those depends on the loop conformation. We may also include side chains on residues in some sphere of influence about the loop. Or we may simply include all of the side chains in the protein. We make no distinction at this stage.

Then, to design a reversible MC move that involves only the loop backbone DoF as well as the selected group  $\mathcal{S}$  of side chains coupled to the loop, we must establish the Metropolis criterion for acceptance of a move of the form

$$\{t_i, \chi_j\} \rightarrow \{t_i + \delta t_i; \chi_j + \delta \chi_j\}, i \in [7, 2N], j \in [1, K] \quad (1)$$

The shape space geometry accessible via our formulation characterizes our moves: assume that the  $L (= 2N)$  torsions for

a loop kinematic chain are divided into the  $L - 6$  controls and 6 compensators. The method used here employs the  $\phi, \psi$  pairs of three amino acids (the *pivots*). These can be chosen at arbitrary locations along the loop, breaking it into three subfragments for kinematic purposes. To each value of the  $L - 6$  controls there correspond up to 16 distinct conformations satisfying the closure conditions, each characterized by a unique set of values of the compensators. As discussed in our earlier work,<sup>26</sup> the 16 alternative solutions represent different orientations of the three subfragments between successive pivots in a reference frame attached to the three pivot  $C\alpha$  atoms about the three axes joining each pair of pivots. Thus, we refer to the method as Triaxial Loop Closure (TLC). The basic idea in the TLC method (discussed more in detail in the next section) is to construct a loop with arbitrary internal degrees of freedom, taking advantage of the fact that the inverse kinematic problem can be solved by determining appropriate values of six torsions. Thus, any variation in the remaining DoF's—other torsions, including  $\Omega$ 's, bond angles, and even bond lengths—can be considered, if so desired. Here, we treated only  $\phi$ – $\psi$  variations, as these are the most “flexible” DoF's, but we could have included all other DoF's in the MC scheme in any combination desired. The conformational variability of the constitutive pieces for loop closure, i.e., the three subfragments, is of course an important factor for solving the closure problem. We see that this variability can be decomposed into two types: the end-to-end variability of the individual fragments and the inherent variability of the loop closure problem, i.e., relative locations and orientations of the ends of the loop as well as the environment in the loop vicinity.

The first is a direct problem: compute the fragment (in practice, we do not check that the fragment is indeed sterically feasible until the assembly is successful). The individual fragment assembly, being subject to no end constraints, is only limited by the Ramachandran and other steric restrictions. However, for purposes of assembling the three subfragments into a self-consistent loop, each individual fragment of length  $L_i$  residues with  $i = 1-3$ , is encoded by four variables: the overall geometric length of the virtual bond joining first and last atoms,  $d_i$ ; the angles  $\theta_i$  and  $\xi_i$  made by the two end bonds to the virtual bond; and the torsion of the two end bonds about the virtual bond,  $\delta_i$ . The variability of the closure problem is governed by these 12 parameters ( $d_i, \theta_i, \xi_i, \delta_i; i = 1-3$ ). The equations expressing closure depend on these parameters smoothly; small changes cause usually small changes in the number and disposition of solutions except that, for certain arrangements, solutions could spontaneously appear or disappear (pairs of polynomial roots may join and become complex, or the converse, see the discussion of the inverse kinematic problem below).

We now search the nearby conformation space by perturbing one of the control torsions. This will result in perturbing the overall structure of one of the chains, leading to a perturbed set of solutions. These changes may lead to overall large motions, see e.g. ref 27 for a discussion of the end conditions and their constraining of various inner DoF. However, a reasonable acceptance ratio for the method can be more or less guaranteed by varying the controls and restricting the step size. Below, we discuss a two-stage scheme, splitting the move into a pure backbone and a pure side chain stage.

**2.3. Solving the Inverse Kinematic Problem.** Many methods for finding solutions that satisfy the closure conditions have been proposed, both exact<sup>18,22,26,28–32</sup> and approximate.<sup>6,21,33–37</sup> Exact methods address the inverse kinematic problem by searching

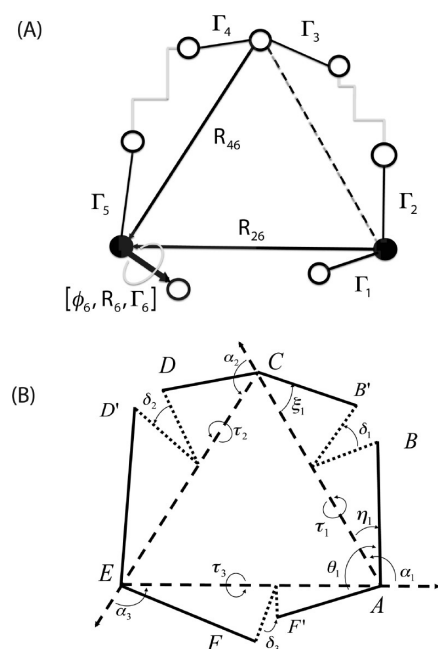


**Figure 1.** (A) The atoms and parameters defining triaxial loop closure (TLC). (B) The generalized 6R/3A kinematic chain.

for the values of a certain torsion, say  $\tau$ , in terms of which all other torsions can be determined. Go and Scheraga<sup>18</sup> pursued a direct solution in the original angle variables. This involves finding the zeros of a certain transcendental expression, a process that may require substantial computation to adequately resolve the entire domain. Subsequent works employ standard techniques from the robotics literature to convert to a more tractable polynomial form in the variable  $u = \tan \tau/2$ . All of the real roots of this 16th degree polynomial can be found efficiently and stably by the use of the method of Sturm chains.<sup>38</sup> All other torsions can be recovered readily, and therefore such methods are capable of finding all backbone solutions for any given combination of control torsion values. On the other hand, approximate methods typically use an iterative procedure to find a solution. As a result, they are not guaranteed to find all solutions consistent with a given set of control values, and the same is true for the approach in ref 18, which is also followed in refs 20, 23, and 24, although for this class of methods the issues are mainly related to the computational sensitivity of multiple roots.

In previous applications the *conrot* algorithm has been used.<sup>20</sup> It places the rotatable bonds on six consecutive bonds plus a driver. A generalization by Wu and Deem<sup>22</sup> uses one driver on either end. A weakness of the *conrot* approach is that a change on either side of the short compensator segment may make the closure problem unsolvable.<sup>24</sup> A generalization from robotics removes that restriction.<sup>29</sup> Our own method for solving the tripeptide closure problem, explained in detail in ref 26, has the advantage of mathematical simplicity, speed, and robustness. It also allows for a straightforward generalization for longer chains of arbitrary geometry. Its simplicity comes from taking advantage of the natural pairing up of rotatable bonds in amino acids to reduce the closure problem to three rotations, and we refer to this as the TLC method.<sup>26</sup> Referring to Figure 1b, we note that each  $C\alpha, C, N, C\alpha$  unit is identified by four variables: the overall geometric length of the virtual bond joining first and last atoms,  $d_i$ ; the angles  $\theta_i$  and  $\xi_i$  made by the two end bonds to the virtual

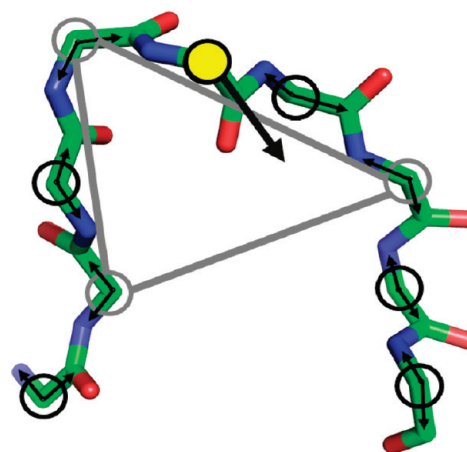


**Figure 2.** Construction of a tripeptide move. A node consists of a  $\phi/\psi$  pair at each  $\alpha$  carbon of the loop (with only backbone shown). The yellow filled circle is the  $\alpha$  carbon, whose dihedral angle serves as a driver angle (the wide black arrow). A randomly constructed triaxial closure is shown as the gray triangle in which each gray circle represents the randomly selected pivot.

bond; and the torsion of the two end bonds about the virtual bond,  $\delta_i$  (actually, the formulation uses the angles  $\alpha_i$  of the triangle formed with edges  $d_i$ ). These definitions remain unchanged even if an arbitrary structure exists between the two end pairs (Figure 1a). We may produce multiple conformations for a long closed chain by partitioning into three subsegments and mapping each to a simple kinematic generalization of the tetrad  $C\alpha, C, N, C\alpha$  (Figure 1a,b).

In brief, three  $C\alpha$  atoms are selected (the pivots). The chain between any two of these, containing  $L$  atoms including the end points, is determined to within a rotation/translation (i.e., in its own body frame) by its own internal coordinates:  $L - 3$  torsions,  $L - 2$  angles,  $L - 1$  lengths. With fixed (to any prescribed value) bond lengths and bond angles, each chain can be completely described by its  $L - 3$  internal torsions. Below, we will index the residues of the three pivots as 1, 2, and 3, and we will index their backbone atoms as  $N_i, C\alpha_i$ , and  $C_i$ ,  $i = 1-3$ , accordingly. Below, we use the atom names interchangeably with their Cartesian coordinates; e.g.,  $N_1$  can be thought of as equivalent to the vector  $\mathbf{R}_1$  etc (see eq 5).

As is explained in ref 26 and somewhat more at length in ref 39 (see also the Supporting Information discussion in ref 40), the three fragments, respectively between pivots 1–2, 2–3, and 3–1, form a triangle with edges  $d_i$ ,  $i = 1-3$ . The parameters necessary for setting up and solving the TLC equations can be extracted from knowledge of only the first two and last two atoms of each chain (Figure 2). Once the three four-atom fragments have been assembled into a triangle, the relative rotation of each fragment about the triangle must place the end atoms relative to those on each neighboring fragment so that the angles ( $N_i, C\alpha_i, C_i$ ,  $i = 1-3$ ) assume prescribed values (Figure 1). In this way, loop closure is accomplished when an appropriate rotation for each piece has been found. It turns out that the problem overlays the solution of a 16th degree polynomial, so that to each real root there corresponds a possible backbone loop geometry (subject, of course, to overall steric viability) to a total of, at most, 16 solutions possible for a given collection of state variables, the control  $2N - 6$  torsions.

**2.4. Jacobian.** Since fixing the end of the chain (the *Closure Conditions*) implies relationships among the torsions, we seek



solution of these relationships such that specifying  $M$  torsions along the loop leads to complete determination of all  $2N$  torsions and unambiguous Cartesian coordinates for all loop backbone atoms that are sterically self-consistent. In general, for any feasible value of the controls, there may exist multiple sets of compensators that allow the loop to close. They are functions of the controls, and their values solve the loop closure problem.

As a result, the element of volume in torsion space, initially uniform in these variables

$$d\mathcal{V} = d\phi_1 d\psi_1 \dots d\phi_N d\psi_N d\chi_1 \dots d\chi_K$$

will need to be modified by

$$dt_1 \dots dt_6 = \frac{\partial(t_1, \dots, t_6)}{\partial(R_6, \Gamma_6, t_6)} dR_6 d\Gamma_6 dt_6$$

leading to the well-known expression (e.g., see formula 23 in ref 23) for the inverse of the above Jacobian:

$$J_i : = J(R_6, \Gamma_6, t_6; t_1, \dots, t_6) = \begin{vmatrix} \Gamma_1 \times \mathbf{R}_{16} & \Gamma_2 \times \mathbf{R}_{26} & \Gamma_3 \times \mathbf{R}_{36} & \Gamma_4 \times \mathbf{R}_{46} & 0 \\ (\Gamma_1 \times \Gamma_6) \cdot \mathbf{e}_1 & (\Gamma_2 \times \Gamma_6) \cdot \mathbf{e}_1 & (\Gamma_3 \times \Gamma_6) \cdot \mathbf{e}_1 & (\Gamma_4 \times \Gamma_6) \cdot \mathbf{e}_1 & (\Gamma_5 \times \Gamma_6) \cdot \mathbf{e}_1 \\ (\Gamma_1 \times \Gamma_6) \cdot \mathbf{e}_2 & (\Gamma_2 \times \Gamma_6) \cdot \mathbf{e}_2 & (\Gamma_3 \times \Gamma_6) \cdot \mathbf{e}_2 & (\Gamma_4 \times \Gamma_6) \cdot \mathbf{e}_2 & (\Gamma_5 \times \Gamma_6) \cdot \mathbf{e}_2 \end{vmatrix} \quad (3)$$

Here

$$\mathbf{R}_{ij} = \mathbf{R}_j - \mathbf{R}_i, \Gamma_i = \frac{\mathbf{R}'_i - \mathbf{R}_i}{\|\mathbf{R}'_i - \mathbf{R}_i\|} \quad (4)$$

and  $\mathbf{e}_i, i = 1-3$ , are the usual unit vectors along axes  $x, y$ , and  $z$  of an arbitrary reference frame (the *Lab frame*). The atoms associated with closure are

$$\mathbf{R}_{2k-1} = N_k, \mathbf{R}_{2k} = C\alpha_k (= \mathbf{R}'_{2k-1}), \mathbf{R}'_{2k} = C_k; \quad k = 1, 2, 3 \quad (5)$$

We note that the term  $\Gamma_5 \times \mathbf{R}_{56} = 0$  and was omitted. In the general case, the three pivot residues are indexed by  $1 \leq n_1 < n_2 < n_3 \leq N$ , and this reindexing will be implied where appropriate.

It is well-known<sup>22</sup> that the Jacobian in the form first proposed by Dodd et al.<sup>20</sup> is incomplete and lacks frame invariance. In a rigorous derivation of the Jacobian from the configuration integral, Wu and Deem<sup>22</sup> show that the correct, frame invariant form is

$$J^{-1} = \frac{1}{\Gamma_6 \cdot \mathbf{e}_3} J_i \quad (6)$$

However, since the acceptance criterion involves ratios of Jacobians computed at the same frame, the additional factors cancel and the relative probabilities remain unchanged.

Although the latter form 6 is indeed invariant if all vectors are changed by an arbitrary affine transformation, it has the undesirable feature that it involves a projection to an arbitrary frame. Consequently, the factor  $\Gamma_6 \cdot \mathbf{e}_3$  may accidentally vanish (in which case  $J_i$  will also vanish), necessitating a random reorientation of the frame to break the degeneracy. Thus, it is desirable to eliminate this superfluous dependence and derive a form that depends only on intrinsic (body frame)

$$J_i = \det \frac{\partial(\mathbf{R}_6, \Gamma_6, t_6)}{\partial t} = \begin{vmatrix} \frac{\partial \mathbf{R}_6}{\partial t_1} & \frac{\partial \mathbf{R}_6}{\partial t_2} & \frac{\partial \mathbf{R}_6}{\partial t_3} & \frac{\partial \mathbf{R}_6}{\partial t_4} & \frac{\partial \mathbf{R}_6}{\partial t_5} & \frac{\partial \mathbf{R}_6}{\partial t_6} \\ \frac{\partial \Gamma_6}{\partial t_1} \cdot \mathbf{e}_1 & \frac{\partial \Gamma_6}{\partial t_2} \cdot \mathbf{e}_1 & \frac{\partial \Gamma_6}{\partial t_3} \cdot \mathbf{e}_1 & \frac{\partial \Gamma_6}{\partial t_4} \cdot \mathbf{e}_1 & \frac{\partial \Gamma_6}{\partial t_5} \cdot \mathbf{e}_1 & \frac{\partial \Gamma_6}{\partial t_6} \cdot \mathbf{e}_1 \\ \frac{\partial \Gamma_6}{\partial t_1} \cdot \mathbf{e}_2 & \frac{\partial \Gamma_6}{\partial t_2} \cdot \mathbf{e}_2 & \frac{\partial \Gamma_6}{\partial t_3} \cdot \mathbf{e}_2 & \frac{\partial \Gamma_6}{\partial t_4} \cdot \mathbf{e}_2 & \frac{\partial \Gamma_6}{\partial t_5} \cdot \mathbf{e}_2 & \frac{\partial \Gamma_6}{\partial t_6} \cdot \mathbf{e}_2 \\ \frac{\partial t_6}{\partial t_1} & \frac{\partial t_6}{\partial t_2} & \frac{\partial t_6}{\partial t_3} & \frac{\partial t_6}{\partial t_4} & \frac{\partial t_6}{\partial t_5} & \frac{\partial t_6}{\partial t_6} \end{vmatrix}$$

Since

$$\frac{\partial \mathbf{R}_k}{\partial t_j} = \Gamma_j \times \mathbf{R}_{jk}, \frac{\partial \Gamma_6}{\partial t_j} = \Gamma_j \times \Gamma_6, \frac{\partial t_i}{\partial t_j} = \delta_{ij} \quad (2)$$

this Jacobian can assume the simpler,  $5 \times 5$  form

coordinates, for which invariance is easily seen. This can be accomplished by carrying out an expansion of this determinant in complementary minors; indeed, the top three rows are expressed in terms of intrinsic coordinates, while the last two involve projections to the space frame. We thus expand the determinant as

$$J_i = \sum_{i=1}^4 (-1)^i \begin{vmatrix} (\Gamma_i \times \Gamma_6) \cdot \mathbf{e}_1 & (\Gamma_5 \times \Gamma_6) \cdot \mathbf{e}_1 \\ (\Gamma_i \times \Gamma_6) \cdot \mathbf{e}_2 & (\Gamma_5 \times \Gamma_6) \cdot \mathbf{e}_2 \end{vmatrix} \begin{vmatrix} \Gamma_j \times \mathbf{R}_{j6} & \Gamma_k \times \mathbf{R}_{k6} & \Gamma_l \times \mathbf{R}_{l6} \end{vmatrix} \quad (7)$$

where the indices  $(i,j,k,l)$  are a cyclic permutation of  $(1,2,3,4)$ .

Applying the well-known identity (e.g., in ref 41, eq 25, p.76)

$$\begin{vmatrix} \mathbf{A} \cdot \mathbf{C} & \mathbf{B} \cdot \mathbf{C} \\ \mathbf{A} \cdot \mathbf{D} & \mathbf{B} \cdot \mathbf{D} \end{vmatrix} = \mathbf{A} \cdot \mathbf{C} \mathbf{B} \cdot \mathbf{D} - \mathbf{B} \cdot \mathbf{C} \mathbf{A} \cdot \mathbf{D} = (\mathbf{A} \times \mathbf{B}) \cdot (\mathbf{C} \times \mathbf{D}) \quad (8)$$

to the first of the  $2 \times 2$  minors in eq 7, we have

$$\begin{vmatrix} (\Gamma_1 \times \Gamma_6) \cdot \mathbf{e}_1 & (\Gamma_5 \times \Gamma_6) \cdot \mathbf{e}_1 \\ (\Gamma_1 \times \Gamma_6) \cdot \mathbf{e}_2 & (\Gamma_5 \times \Gamma_6) \cdot \mathbf{e}_2 \end{vmatrix} = (\Gamma_1 \times \Gamma_6) \times (\Gamma_5 \times \Gamma_6) \cdot \mathbf{e}_3 = (\Gamma_1 \cdot \Gamma_5 \times \Gamma_6)(\Gamma_6 \cdot \mathbf{e}_3)$$

The remaining  $2 \times 2$  minors result in analogous expressions. Substituting these into eq 7, we have

$$\frac{J_i}{\Gamma_6 \cdot \mathbf{e}_3} = \sum_{i=1}^4 (-1)^i (\Gamma_i \cdot \Gamma_5 \times \Gamma_6) \begin{vmatrix} \Gamma_j \times \mathbf{R}_{j6} & \Gamma_k \times \mathbf{R}_{k6} & \Gamma_l \times \mathbf{R}_{l6} \end{vmatrix} \quad (10)$$

(as above, the indices  $(i,j,k,l)$  are a cyclic permutation of  $(1,2,3,4)$ ), which can be recombined to give the expression

for the inverse Jacobian

$$J^{-1} = \frac{1}{\Gamma_6 \cdot \mathbf{e}_3}$$

$$J_i = \begin{vmatrix} \Gamma_1 \times \mathbf{R}_{26} & \Gamma_2 \times \mathbf{R}_{26} & \Gamma_3 \times \mathbf{R}_{46} & \Gamma_4 \times \mathbf{R}_{46} \\ (\Gamma_1 \cdot \Gamma_5 \times \Gamma_6) & (\Gamma_2 \cdot \Gamma_5 \times \Gamma_6) & (\Gamma_3 \cdot \Gamma_5 \times \Gamma_6) & (\Gamma_4 \cdot \Gamma_5 \times \Gamma_6) \end{vmatrix} \quad (11)$$

where we took advantage of the fact that  $\Gamma_i \times \mathbf{R}_{i6} = \Gamma_i \times \mathbf{R}_{i+1,6}$  with  $i = 1$  and  $3$  due to the fact that the axes  $\Gamma_i$  and  $\Gamma_{i+1}$ ,  $i = 1$  or  $3$ , are coterminal. Figure 1a shows all quantities that enter in the Jacobian.

This  $4 \times 4$  determinant is the frame invariant form of the inverse Jacobian for the TLC method. It has the advantage that it is expressed entirely in terms of body coordinates, and thus it is free from degeneracies and can be evaluated without projecting to an ad hoc coordinate system. It is numerically equivalent to the Wu and Deem form 6, when the latter is defined. The Jacobian 11 can be easily expressed in terms of the intrinsic parameters  $(d_i, \theta_i, \xi_i, \delta_i)$ ,  $i = 1-3$ , entering in the TLC algorithm,<sup>42</sup> a feature that it shares with reduced Jacobians derived by other authors.<sup>22,43</sup> However, such expressions lack the simplicity and geometrical appeal of eq 11.

**2.5. Backbone Perturbation Procedure.** The loop closure algorithm described in the previous section, while perfectly general, is currently implemented as a strategy for perturbing only the backbone coordinates. The side chain coordinates perturbation procedure, as well as the strategy for combining these perturbations in a way such that detailed balance is maintained, will be outlined in the next two sections. An important design feature of this approach is that the backbone and side chain perturbations are generated independently.

An important feature of both the backbone selection probability and the side chain selection probability is that they are reversible, or

$$\alpha(\mathbf{t} \rightarrow \mathbf{t}') = \alpha(\mathbf{t}' \rightarrow \mathbf{t}) \quad (12)$$

where  $\mathbf{t}' = \mathbf{t} + \delta\mathbf{t}$  is the trial move starting from the torsion state  $\mathbf{t}$  and  $\delta\mathbf{t}$  is the perturbation vector to the loop of interest. For the purposes of this work, we require the selection probability to be uniform to enforce eq 12. For this to be true, we need to establish the procedure which ensures that a uniform distribution of torsions over the entire loop can be generated.

The procedure for generating a trial move  $\delta\mathbf{t}$  closely follows that of refs 20, 22, 23, and 29. Since the algorithm currently solves for  $2N - 6$  torsions, and we wish to have a procedure that is valid for loops of arbitrary length, we must select a subset of  $2N - 6$  torsions. There is some flexibility in how this could be done, but the present implementation is as follows (see Figure 2):

- (1) From the designated loop torsions, a single torsion angle  $i$  is selected uniformly and identified as a driver angle coordinate (the yellow circle in Figure 2), as has been described in previous work.<sup>26</sup>
- (2) For torsion  $t_i$ , a random variate  $\delta t_i$  is generated, with a maximum value of up to  $\pi$ .
- (3) A randomly constructed triaxial closure is generated by randomly selecting three  $\alpha$  carbons as pivots from the loop (excluding the  $\alpha$  carbon on which the driver angle resides) and assigning the  $\phi/\psi$  angles as the torsions (the gray triangle in Figure 2).

- (4) A set of torsions for the stationary solution  $\mathbf{t}_k$ ,  $k \in [1, K]$ , is generated, resulting in up to  $K = 16$  solutions. For this case, only the alternative sets of pivot coordinates are considered, with the driver angle held at  $t_i$ . For each solution, a Jacobian term  $J(\mathbf{t}_k)$  is computed.
- (5) A set of torsions for the perturbed solution  $\mathbf{t}_l$ ,  $l \in [1, L]$ , is similarly generated, with associated  $J(\mathbf{t}_l)$  terms.
- (6) A trial solution  $\mathbf{t}'$  is selected from the solutions  $(\mathbf{t}_k, \mathbf{t}_l)$  with the following probability:

$$\alpha(\mathbf{t} \rightarrow \mathbf{t}') = \frac{J(\mathbf{t}')}{\sum_{k=1}^K J(\mathbf{t}_k) + \sum_{l=1}^L J(\mathbf{t}_l)} \quad (13)$$

To show that this procedure generates a uniform distribution, the  $\phi/\psi$  angles of an 11-residue polypeptide is sampled with no potential. Half of the time, the loop closure procedure is applied as described above, and the other half of the time, only a driver angle is perturbed uniformly, with the remaining Cartesians updated accordingly (with no closure condition enforced). The second procedure is required so that the full space of dihedral angles is accessible. Every move is accepted, with no potential applied or steric exclusion. This procedure generates a uniform distribution of torsions, as is shown in Figure 3. It shows a distribution of an 11-residue peptide sampled with the loop closure procedure described above. Only backbone DoF are sampled, and no force field is applied. The end points are constrained to fixed positions. This control closely follows previous work.<sup>20,23</sup> Figure 3a shows the distribution of angles with no Jacobian selection term applied, and Figure 3b shows the distribution with the reweighting term applied. The Jacobian term clearly improves the uniformity of the sampling.

**2.6. Side Chains.** The efficient sampling of side chains<sup>22</sup> is important since side chain conformations often determine the biological function of proteins. In the current work, the side chain  $\chi$  angles are not taken from the rotamer library due to their nonuniform distribution. Instead, to generate the side chain trial moves, a single side chain is randomly selected, and each  $\chi$  angle is perturbed by a value which is randomly and uniformly distributed in a defined domain  $[-d/2, d/2]$ .<sup>25,44</sup> The polar hydrogens for the selected residue are sampled as well over the domain  $[-\pi, \pi]$ .

To improve the sampling efficiency, no energy is computed for the states with steric clashes, which are defined on the basis of the distances between heavy atoms. Specifically, a steric clash is defined when pairs of heavy atoms are closer than 0.7 times the sum of their Lennard-Jones radii. Rapid identification of steric clashes (using neighbor lists) avoids computationally expensive energy evaluations, for conformations that will result in very high energies and negligible acceptance probabilities.

The most expensive term in energy evaluation is the solvation energy in which the time-consuming step is the computation of Born radii. Since the Born radii and the long-range energy terms generally vary slowly for relatively small, local conformational changes, less frequent evaluation of these terms will contribute more to the sampling performance. For this purpose, the multiple time-step Monte Carlo sampling (MTSMC) procedure<sup>45</sup> is incorporated in the present method, in a scheme based on that in ref 44. The Born radii and the long-range interactions are held fixed at the latent state of the original coordinates during the

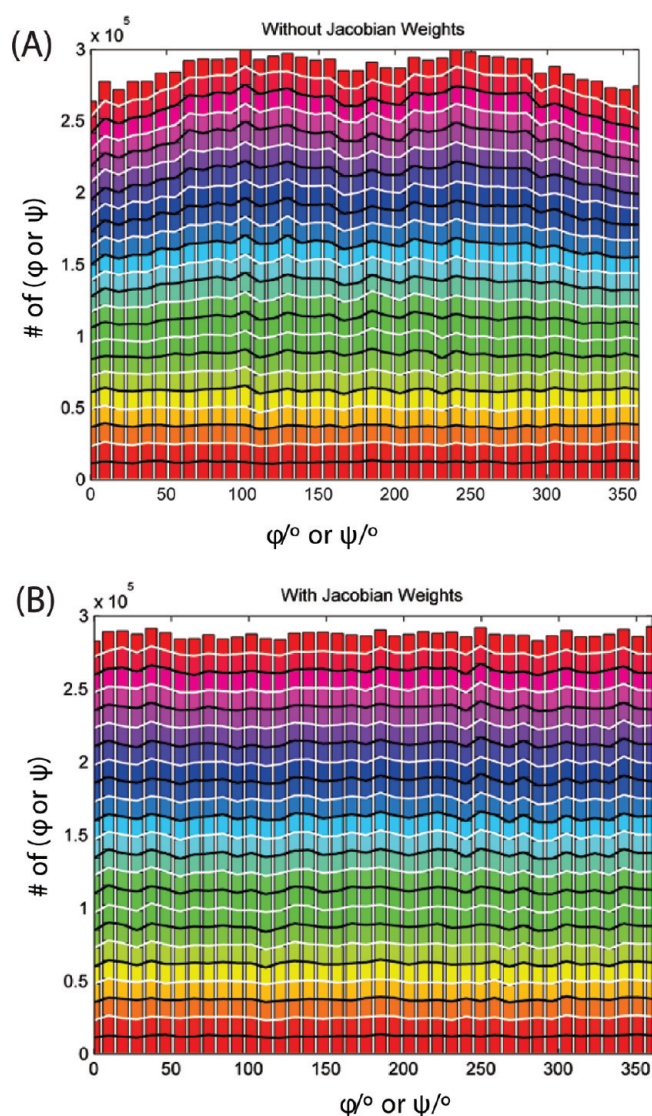


**Figure 3.** Distribution of  $\phi/\psi$  angles without (A) and with (B) Jacobian weighting of selection for an 11-residue peptide. A total of  $4.5 \times 10^5$  trial moves were generated. No force field is used in the selection probability, and all trial moves are accepted.

inner loop sampling and only updated in every outer loop calculation. The final configuration from the inner loop is then taken to be a trial move and subjected to the MTSMC acceptance criterion (see eq 20 in ref 25).

**2.7. The POSH Monte Carlo Method.** Both the TLC method for determining the backbone moves of loop residues and the side chain sampling via perturbation have been incorporated in the POSH (port out, starboard home) Monte Carlo method introduced in a previous work.<sup>25</sup> The application of this method on small peptide systems has shown reasonable agreement with experiments.<sup>25</sup> In the present work, we are interested in its performance in more complicated protein systems with flexible loops.

Briefly, the move sets in this approach consist of two steps: an initial trial ( $1 \rightarrow 2$ ) move with large perturbation followed by a series of annealing moves consisting of smaller perturbation within the inner loop of length  $N_I$  ( $2 \rightarrow 3$ ). The generalized Metropolis acceptance probability for this series of moves is

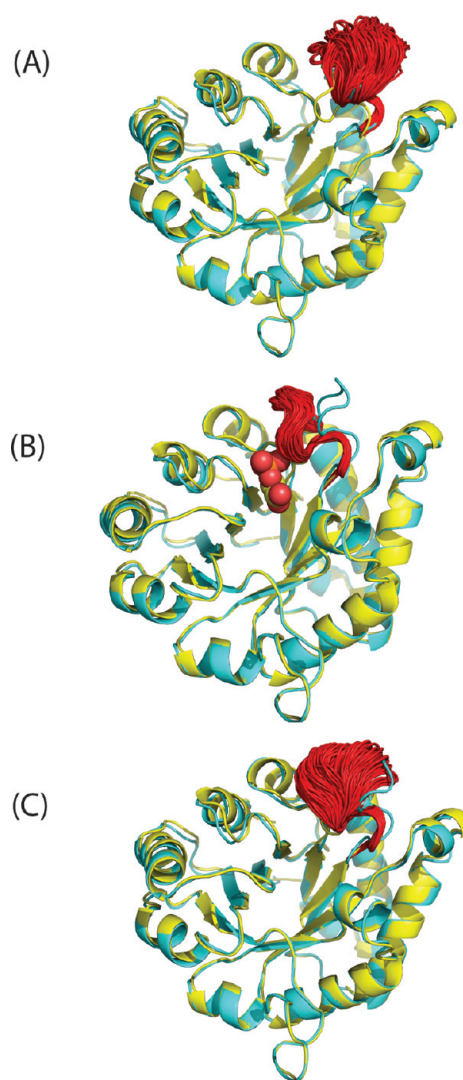


**Figure 4.** The ensemble structures (red) for the flexible loop (residues 165–178) of yeast TIM were taken from the equilibrium simulation with initial structures of (A) the apo (open) conformation, (B) the bound (closed) conformation, and (C) the closed conformation with the ligand PGA removed. The X-ray structure of apo yeast TIM (PDB 1YPI) is shown in yellow and the bound state (PDB 2YPI) in cyan. The ligand PGA is depicted by spheres.

given by

$$acc(1 \rightarrow 3) = \min \left( 1, \frac{p_3 T_{41}}{p_1 T_{23}} \right) \quad (14)$$

where  $p_1$  and  $p_3$  are the probabilities of being in the original and final trial state, respectively.  $T_{41}$  and  $T_{23}$  are transition probabilities.  $T_{23}$  is the normal forward transition probability, as would be given in the usual derivation of detailed balance, but  $T_{41}$  is a reverse transition probability that is constructed using an alternative reverse path through configuration space that is constructed by taking the final state (state 3) and subtracting the perturbation ( $1 \rightarrow 2$ ) from state 3 to arrive at state 4. Further details are given in ref 25.

The trial moves are generated by a perturbation that uniformly varies over some domain  $[-d/2, d/2]$  with a different magnitude for the initial and annealing steps. In this work, for both types of



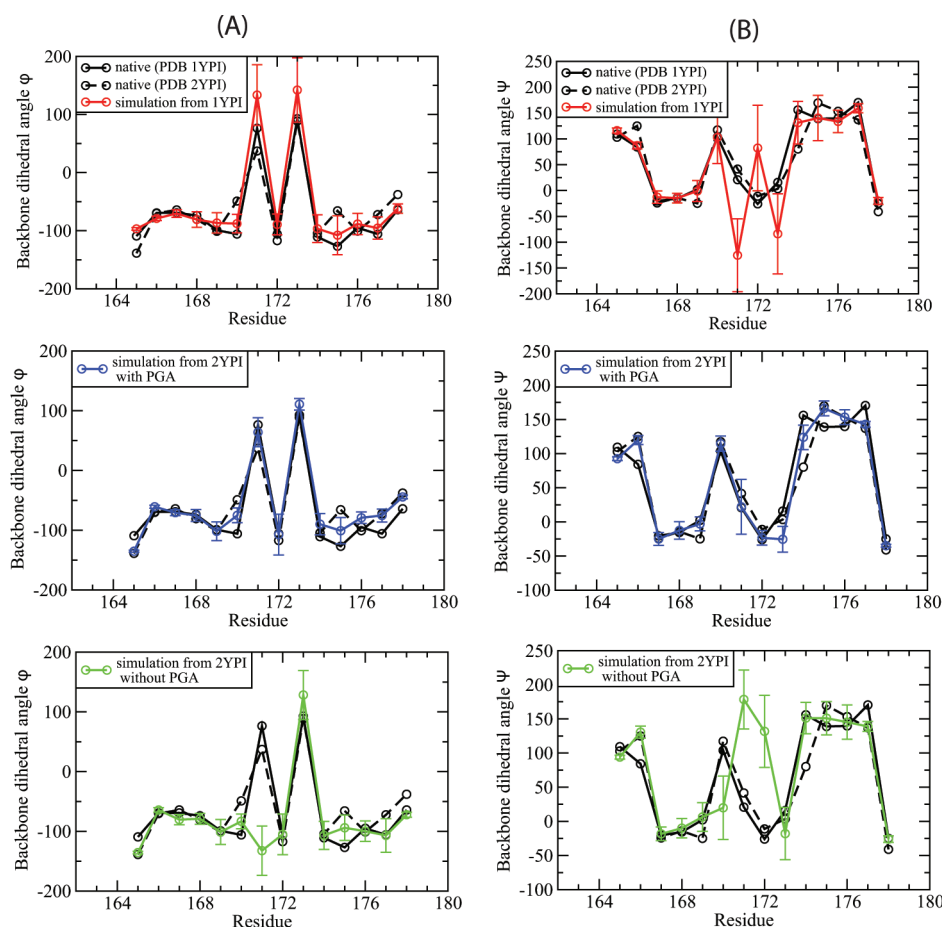


**Figure 5.** Comparison of the calculated backbone dihedral angles,  $\phi$  (A) and  $\psi$  (B), with those measured in the X-ray structures. The black solid line is for apo TIM (PDB 1YPI) and the dashed line for the ligand-bound TIM (PDB 2YPI). The calculated dihedral angles were averaged over the equilibrium ensemble simulated from the initial structure of apo (red), ligand-bound (blue), and closed forms with the ligand PGA removed (green).

trial moves, either the backbone or side chain is allowed to be perturbed with equal probability. For backbone perturbations, the  $\phi$  or  $\psi$  dihedral angle can vary over the domain of  $[-2\pi, 2\pi]$  for initial steps and  $[-\pi/4, \pi/4]$  for annealing steps. For side chain  $\chi$  angles, the domains are  $[-\pi, \pi]$  and  $[-\pi/9, \pi/9]$ , respectively, for the initial and inner step trial moves. The number of inner steps  $N_I$  is set to 20, which was reported as the upper bound of inner steps for generating precise distribution. For all protein systems studied in this work, a mixture of 50% POSH and 50% standard MC sampling, followed by the MTSMC procedure, is used due to its better performance as studied in the previous work.<sup>25</sup>

### 3. SIMULATIONS

We applied the loop Monte Carlo method described above to several proteins with flexible loops. The first is the enzyme triosephosphate isomerase (TIM), which has been used as a model system for studying loop flexibility, primarily by NMR. This enzyme catalyzes the reversible isomerization of dihydroxyacetone phosphate (DHAP) to D-glyceraldehyde 3-phosphate (GAP). The active site loop 6 (residues 167–176) undergoes conformational changes upon ligand binding and is believed to be flexible in the absence of ligand binding, transitioning between “open” and “closed” states. To assess the capability of our

method to capture the dynamical properties of this flexible loop, three sets of simulations were performed. The first one started from the apo yeast TIM (PDB ID 1YPI) with an open loop conformation (we call this SIM1). The second started from the 2-phosphoglycolate (PGA)-bound TIM (PDB ID 2YPI) with the closed loop conformation (SIM2), and the third is the same as the second except that the ligand PGA was removed from the initial structure (SIM3).

The titratable residues in the starting structures were predicted according to the experimental conditions. Specifically, in all simulations, His95 was treated as neutral and protonated on the N  $\in$  2. Glu165 is protonated in SIM2 in order to maintain the strong interaction with ligand PGA<sup>9</sup> but was unprotonated in the other simulations. Residues within 8 Å of the active site loop were included for the side chain sampling, and the flexible loop was extended to include residues 165–178 in the simulations for both the backbone and side chain sampling. The force field OPLS-AA<sup>46,47</sup> was used for the protein TIM and ligand PGA except that the partial charges for the phosphate group of PGA were adjusted on the basis of the previous work by Wong et al.<sup>48</sup> The surface generalized Born (SGB)<sup>49,50</sup> model was used for implicit solvent with the treatment of nonpolar terms.<sup>50</sup> To prevent the sampling from being trapped in local minima, all simulations were performed at a temperature of 600 K. Each simulation has a length of  $N_o = 2 \times 10^5$  up to  $5 \times 10^5$  outer steps. Data analyses were performed over

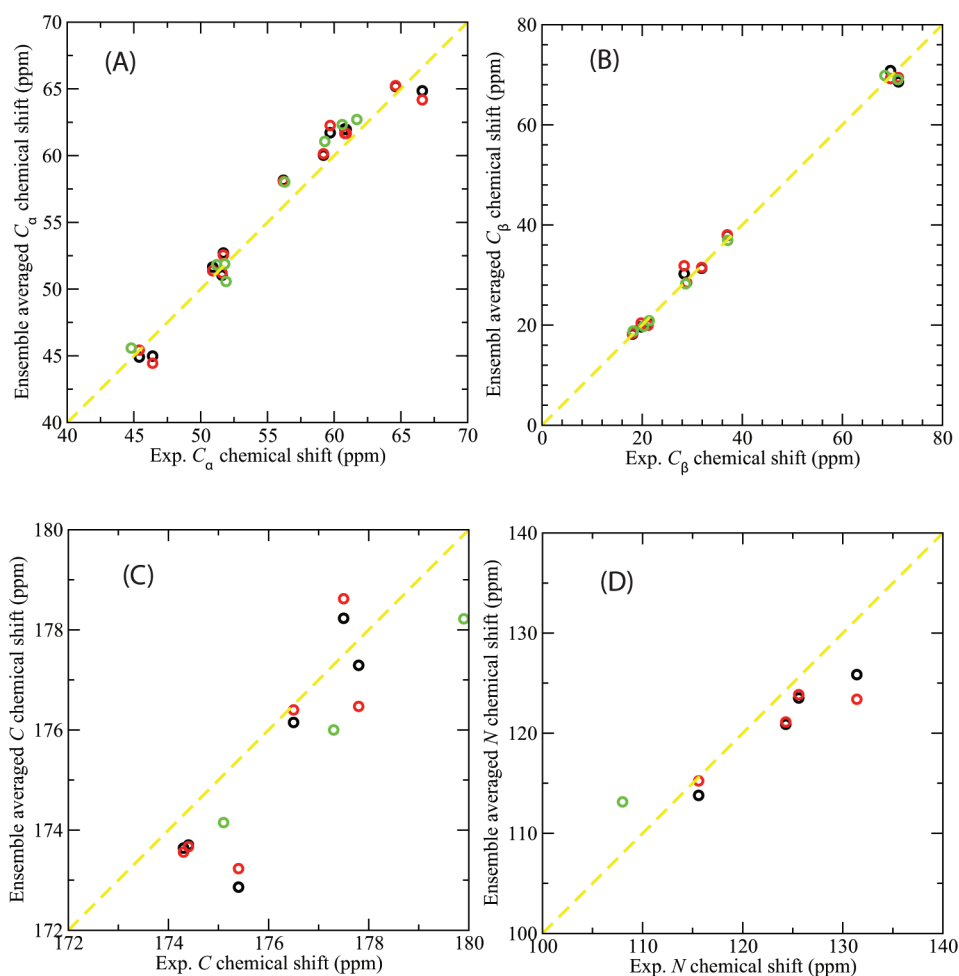


**Figure 6.** Ensemble-averaged chemical shifts (ppm) versus the NMR experimental measurements for  $C_{\alpha}$  (A),  $C_{\beta}$  (B), carbonyl C (C), and amide N (D) atoms of the flexible loop 6 of yeast TIM. SHIFTX<sup>56</sup> was used to calculate chemical shifts, which were then averaged over an ensemble of 1000 structures from the equilibrated MC simulations. The starting PDB structures for the simulations are 1YPI (black), 2YPI with the ligand PGA removed (red), and 2YPI with PGA bound (green). The experimental chemical shift data are those for apo yeast TIM in the NMR experiment<sup>57</sup> (for comparison with the apo simulations), and for yeast TIM with ligand G3P<sup>57</sup> (for comparison with the holo simulation). Experimental chemical shifts are not available for some atoms, and these are omitted.

the equilibrium simulations (roughly after  $10^5$  outer steps) during which the potential energy is relatively stable.

The same protocol was also applied to other protein systems which have been studied by NMR experiments, specifically those with PDB ID 1H2O, 1XWE, and 1Q9P. By choosing NMR structures, we eliminate any concerns about crystal packing influencing the loop conformation or flexibility. These specific proteins were chosen because each has two loops consisting of 5–8 residues, one of which has multiple conformations with large variation among the various NMR models (flexible loop) and the other has a narrow range of loop conformations among the NMR models (rigid loop). Both the flexible and rigid loops were simulated using the same sampling protocol and the same parameter settings in order to compare with the experimental data since both loops within the same protein were measured under the same experimental conditions. The titratable residues in the starting structures were protonated at the experimental pH = 7.0 for 1H2O, 6.0 for 1XWE, and 5.8 for 1Q9P. The flexible loops consist of residues 59–64 for 1H2O, 1609–1616 for 1XWE, and 48–53 for 1Q9P; the residues in the rigid loops are 46–51 for 1H2O, 1536–1540 for 1XWE, and 78–82 for 1Q9P.

## 4. RESULTS AND DISCUSSION

As an initial illustration of the utility of our loop MC method for sampling the conformation space of protein loops, we applied this method to the well-studied enzyme triosephosphate isomerase (TIM). The active site loop undergoes large-scale motions interconverting between open and closed conformations. This conformational transition occurs on the time scale of milliseconds,<sup>17</sup> making it a challenge for molecular dynamics simulations in previous studies.<sup>51,52</sup>

In the current work, multiple transitions between open and closed loop conformations of yeast TIM have been observed in the simulation of the apo protein, but only at 600 K (vide infra). Figure 4a and c, which start from the open and closed state, respectively, show sampled loop conformations from the equilibrium ensemble, spanning both the open and closed form. In the simulation with the ligand PGA bound, the active site loop stays in the closed conformation, as can be seen in Figure 4b. These results agree qualitatively with NMR experiments, which found that the loop samples open and closed conformations whether or not a ligand was bound, but ligand binding shifted the



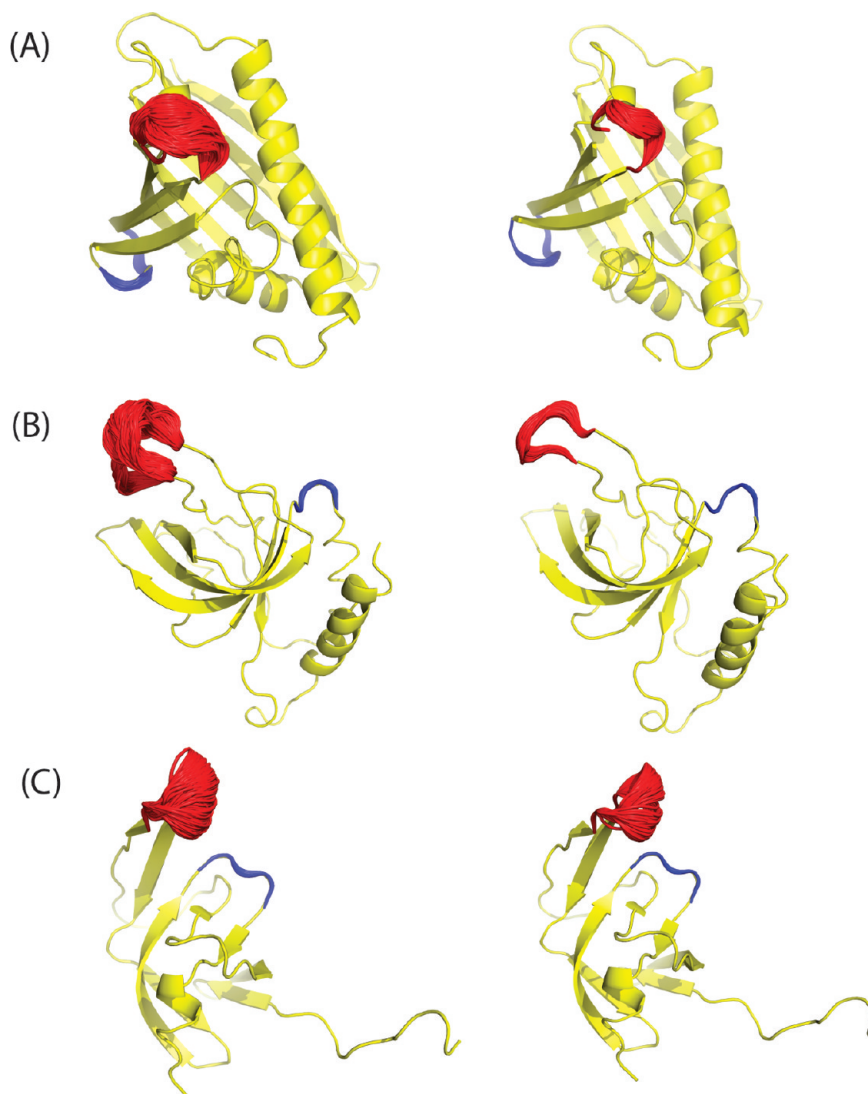


**Figure 7.** Ensembles of loop structures from equilibrium simulations using MC sampling for proteins with PDB ID (A) 1H2O, (B) 1XWE, and (C) 1Q9P sampled at  $T = 600$  K (left) and  $T = 300$  K (right). The sampled flexible loops (“floppy”) which have a large fluctuation in the NMR models are shown in red, and the rigid loops with very small fluctuations are in blue. The structures in yellow are taken from MODEL 1 of the PDB file.

equilibrium strongly toward the closed conformation.<sup>17,53</sup> Upon PGA binding, the carboxylate of the ligand protonates residue Glu165, making it hydrogen bonded with PGA instead of with Ser96 in the apo structure, such that the closed loop conformation is preferred in the presence of a ligand.

It has been known that the active site loop of TIM moves largely as a rigid unit.<sup>51,54</sup> Figure 5 shows that the backbone dihedral angles of the flexible loop in the X-ray structure of apo TIM are very similar to those in the structure of ligand-bound TIM. The ensembles generated by the loop MC method largely agree with the experimental data in this regard. We calculated the backbone  $\phi$  and  $\psi$  angles and averaged them over the equilibrium ensemble for each of the three simulations. For the holo simulations, the ensemble averaged  $\phi$  and  $\psi$  angles agree well with those measured in the X-ray structures, as shown in Figure 5a and b (blue lines). Similar agreement was also found for the apo simulations started from both the open and closed conformations, except that residues 170–173 have relatively large deviations and fluctuations, which is consistent with the

findings in previous simulation studies<sup>17,52</sup> (red and green lines in Figure 5a and b).

NMR spectroscopy can provide information on both the structure and dynamics of proteins in physiologically relevant environments.<sup>55</sup> The chemical shift is NMR’s most ubiquitous parameter, the variation of nuclear magnetic resonance frequencies of the same kind of nucleus being due to variations in the electron distribution. To directly compare with the experimental data, ensemble averaged chemical shifts were calculated for each equilibrium ensemble using SHIFTX<sup>56</sup> to calculate chemical shifts for the residues of the flexible loop in each conformation and then averaging over all of the conformations in the ensemble. For the apo simulations, starting from either the open or closed structures, the ensemble-averaged chemical shifts were compared with NMR measurements of apo yeast TIM.<sup>57</sup> For the simulation of the ligand-bound, closed structure, NMR data measured for G3P-bound yeast TIM<sup>57</sup> were used. [The chemical shifts for the closed loop of the enzyme bounded with G3P and GPA are very similar (Yimin Xu, personal communication).]

**Table 1. Root-Mean-Squared Fluctuation (RMSF; Å) of Heavy Atoms of Both Floppy and Rigid Loops in the Equilibrium Ensemble Simulated by POSH MC Method with Initial Structure of the First Model of NMR Structures<sup>a</sup>**

heavy atom RMSF	1H2O			1Q9P			1XWE		
	POSH			POSH			POSH		
	NMR	600 K	300 K	NMR	600 K	300 K	NMR	600 K	300 K
flexible loop	2.75	1.64	0.75	3.51	1.27	1.06	4.83	2.50	1.10
rigid loop	0.49	0.40	0.15	1.25	0.38	0.18	1.03	0.50	0.31

<sup>a</sup> For comparison, the RMSFs over all NMR models for each protein are also computed at both 600 and 300 K.

A strong linear correlation was found between the ensemble-averaged and experimentally measured chemical shifts for C $_{\alpha}$  (Figure 6a) and C $_{\beta}$  (Figure 6b) atoms with a correlation coefficient  $r$  of 0.98 or higher in all cases. For carbonyl C and amide N atoms of the flexible loop, although there are fewer experimental chemical shifts available, the calculated ensemble averages have small variations from experimental values (Figure 6c and d). The agreement with the NMR chemical shifts provides additional evidence that the ensembles generated by the loop MC sampling are reasonable.

We note that the experimental chemical shifts were measured at 300 K, while our simulations were performed at 600 K. This is because at 300 K it is difficult to observe the conformational transitions between the open and the closed state. We suspect, but cannot prove, that this occurs in part due to (1) the well-known tendency of generalized Born implicit solvent models to overstabilize salt bridges, (2) the effect of constraining the  $\Omega$  angles, as well as the bond angles and lengths, in addition to the loop closure condition, and (3) sampling only the loop and not the remainder of the protein. Using a higher temperature overcomes all of these effects, and reasonable ensembles are generated which agree with the NMR chemical shifts. Because the Monte Carlo sampling scheme does not perturb degrees of freedom outside the loop, such that the overall structure is preserved, a higher temperature sampling protocol can still provide physical insights. The efficiency gained by sampling a lower dimensional space, while still obtaining a reasonable estimate of ensemble properties, motivates the use of this set of approximations.

As a second initial application, we also applied our sampling method to other protein structures, solved by NMR, which have loops with differing flexibilities in order to evaluate our ability to distinguish the flexible and rigid loops within the same protein. The conformational ensembles from equilibrium simulations for both the flexible and rigid loops are shown in Figure 7 for three proteins with PDB ID 1H2O (a), 1XWE (b), and 1Q9P (c) sampled at 600 K (left) and 300 K (right). These results clearly show that the loop residues which are flexible in the experimentally derived structures consistently are more floppy in the sampled ensemble at either temperature than the loop residues, which are relatively rigid in the same NMR structures. To further quantify these results, root-mean-square fluctuations (RMSF) of the heavy atoms in both loops were calculated for the sampled and NMR models, as shown in Table 1. We recognize that the set of NMR models for each protein cannot be viewed as a true ensemble, but the qualitative agreement is nonetheless

encouraging. Thus, for studying protein loop flexibility, our method is a viable alternative to molecular dynamics simulations, which have also been used successfully to obtain ensembles in quantitative agreement with NMR data. In the cases examined here, the differences in rigidity appear to be related simply to the level of solvent exposure; i.e., floppy loops are more solvent exposed and have less interaction with their neighbors. For simulations of all studied protein systems, three NMR targets and TIM, the average acceptance ratio is about 14%.

Our current approach only varies  $\phi$ – $\psi$  angles, as they are most flexible, but actually it is possible to include all other DoF in the MC scheme in any desired combination. We are working on a further version of the algorithm that will incorporate sampling which allows  $\Omega$  angles, as well as bond lengths and angles, to fluctuate more freely, which may allow for lower temperature sampling of systems of this type. Although in the present study we have considered solvation effects implicitly only, including water molecules explicitly in the simulation is possible in principle. However, water molecules in the immediate vicinity of a loop would lead to steric clashes whenever a large backbone move was attempted, which would reduce the efficiency of the present approach.

## AUTHOR INFORMATION

### Corresponding Author

\*Tel.: (415) 514-9811. E-mail: Matt.Jacobson@ucsf.edu.

### Author Contributions

<sup>§</sup>Jerome Nilmeier and Lan Hua contributed equally to this work.

## ACKNOWLEDGMENT

This work was supported in part by grants from NIH-NIGMS, GM081710 (to M.P.J. and E.A.C.), GM086602 (to M.P.J.), and R01-GM090205 (E.A.C.). M.P.J. is a consultant to Schrodinger LLC.

## REFERENCES

- (1) Jones, D. *Curr. Opin. Struct. Biol.* **1997**, *7*, 377.
- (2) Fiser, A.; Do, R.; Sali, A. *Protein Sci.* **2000**, *9*, 1753.
- (3) Al-Lazikani, B.; Jung, J.; Xiang, Z.; Honig, B. *Curr. Opin. Struct. Biol.* **2001**, *5*, 51.
- (4) Jacobson, M. P.; Pincus, D.; Rapp, C.; Day, T.; Honig, B.; Shaw, D.; Friesner, R. *Proteins* **2004**, *55*, 351.
- (5) Meirovich, H. *Chem. Phys. Lett.* **1977**, *45*, 389.
- (6) Baysal, C.; Meirovich, H. *J. Phys. Chem. A* **1997**, *101*, 2185.
- (7) Mihailescu, M.; Meirovitch, H. *J. Phys. Chem. B* **2009**, *113*, 7950.
- (8) Lolis, E.; Abler, T.; Davenport, R.; Rose, D.; Hartman, F.; Petsko, G. *Biochemistry* **1990**, *29*, 6609.
- (9) Lolis, E.; Petsko, G. *Biochemistry* **1990**, *29*, 6619.
- (10) Dar, A.; Lopez, M.; Shokat, K. *Chem. Biol.* **2008**, *15*, 1015.
- (11) Padlan, E. *Adv. Protein Chem.* **1996**, *49*, 57.
- (12) Xu, J.; Davis, M. *Immunity* **2000**, *13*, 37.
- (13) Wong, S.; Jacobson, M. P. *Proteins* **2010** in press.
- (14) Rapp, C.; Pollack, R. *Proteins* **2005**, *60*, 103.
- (15) Wong, S.; Jacobson, M. P. *Proteins* **2008**, *71*, 153.
- (16) Yi, M.; Tjong, H.; Zhou, H. *Proc. Natl. Acad. Sci. U.S.A.* **2008**, *105*, 8280.
- (17) Massi, F.; Wang, C.; Palmer, A. G. *Biochemistry* **2006**, *45*, 10787.
- (18) Go, N.; Scheraga, H. *Macromolecules* **1970**, *3*, 178.
- (19) Brucoleri, R. E.; Karplus, M. *Macromolecules* **1985**, *18*, 2767.
- (20) Dodd, L. R.; Boone, T. D.; Theodorou, D. N. *Mol. Phys.* **1993**, *78*, 961.

- (21) Deem, M.; Bader, J. *Mol. Phys.* **1996**, *87*, 1245.
- (22) Wu, M. G.; Deem, M. W. *Mol. Phys.* **1999**, *97*, 559.
- (23) Dinner, A. J. *Comput. Chem.* **2000**, *21*, 1132.
- (24) Ulmschneider, J. P.; Jorgensen, W. L. *J. Chem. Phys.* **2003**, *118*, 4261.
- (25) Nilmeier, J.; Jacobson, M. P. *J. Chem. Theory Comput.* **2009**, *5*, 1968.
- (26) Coutsiias, E. A.; Seok, C. L.; Jacobson, M. P.; Dill, K. A. *J. Comput. Chem.* **2004**, *25*, 510.
- (27) Hayward, S.; Kitao, A. *Biophys. J.* **2010**, *98*, 1976.
- (28) Wedemeyer, W. J.; Scheraga, H. A. *J. Comput. Chem.* **1999**, *20*, 819.
- (29) Wu, M. G.; Deem, M. W. *J. Chem. Phys.* **1999**, *111*, 6625.
- (30) Cortes, J.; Simeon, T.; Remaud-Simeon, M.; Tran, V. *J. Comput. Chem.* **2004**, *25*, 956.
- (31) Noonan, K.; O'Brien, D.; Snoeyink, J. *Int. J. Robotics Res.* **2005**, *24*, 971.
- (32) Milgram, R.; Liu, G.; Latombe, J. J. *Comput. Chem.* **2008**, *29*, 50.
- (33) Favrin, G.; Irbäck, A.; Sjunnesson, F. *J. Chem. Phys.* **2001**, *114*, 8154.
- (34) Wang, L.-C. T.; Chen, C. C. *IEEE Trans Robot. Autom.* **1991**, *7*, 489.
- (35) Cahill, S.; Cahill, M.; Cahill, K. J. *Comput. Chem.* **2003**, *24*, 1364.
- (36) Canutescu, A.; Dunbrack, R. *Protein Sci.* **2003**, *12*, 963.
- (37) Lee, A.; Streinu, I.; Brock, O. *Phys Biol* **2005**, *2*, 108.
- (38) Stoer, J.; Bulirsch, R. *Numerical Analysis*, 2nd ed.; Springer: Berlin, 1991.
- (39) Coutsiias, E. A.; Seok, C.; Wester, M. J.; Dill, K. A. *Int J. Quant. Comp.* **2006**, *106*, 176.
- (40) Mandell, D. J.; Coutsiias, E. A.; Kortemme, T. *Nature Methods* **2009**, *6*, 551.
- (41) Gibbs, J. W.; Wilson, E. B. *Vector Analysis*, 1st ed.; Yale University Press: New Haven, CT, 1901.
- (42) Pollock, S. N.; Coutsiias, E. A. *Numerical Analysis of Inverse Kinematic Algorithms*, preprint, 2011.
- (43) Hoffman, D.; Knapp, E.-W. *Eur. Biophys. J.* **1996**, *24*, 387.
- (44) Nilmeier, J.; Jacobson, M. P. *J. Chem. Theory Comput.* **2008**, *4*, 835.
- (45) Hetenyi, B.; Bernacki, K.; Berne, B. J. *J. Chem. Phys.* **2002**, *117*, 8203.
- (46) Kaminski, G. A.; Friesner, R. A.; Tirado-Rives, J.; Jorgensen, W. L. *J. Phys. Chem. B* **2001**, *105*, 6474.
- (47) Jorgensen, W.; Maxwell, D.; Tirado-Rives, J. *J. Am. Chem. Soc.* **1996**, *118*, 11225.
- (48) Wong, S.; Bernacki, K.; Jacobson, M. P. *J. Phys. Chem. B* **2005**, *109*, 5249.
- (49) Ghosh, A.; Rapp, C.; Friesner, R. J. *J. Phys. Chem. B* **1998**, *102*, 10983.
- (50) Gallicchio, E.; Zhang, L.; Levy, R. J. *Comput. Chem.* **2002**, *23*, 517.
- (51) Joseph, D.; Petsko, G.; Karplus, M. *Science* **1990**, *249*, 1425.
- (52) Derreumaux, P.; Schlick, T. *Biophys. J.* **1998**, *74*, 72.
- (53) Williams, J. C.; McDermott, A. E. *Biochemistry* **1995**, *34*, 8309.
- (54) Davenport, R.; Bash, P.; Seaton, B.; Karplus, M.; Petsko, G.; Ringe, D. *Biochemistry* **1991**, *30*, 5821.
- (55) Teng, Q. Protein Structure Determination from NMR Data. In *Structural Biology: Practical NMR Applications*, 1st ed.; Lee, W., Ed.; Springer: Berlin, 2005.
- (56) Neal, S.; Nip, A.; Zhang, H.; Wishart, D. J. *Biomol. NMR* **2003**, *3*, 215.
- (57) Xu, Y.; Lorieau, J.; McDermott, A. E. *J. Mol. Biol.* **2010**, *397*, 233.